

# Non-perturbative signatures of fractons in the twisted multi-flavor Schwinger Model

Pavel P. Popov,<sup>1,\*</sup> Valentin Kasper,<sup>1</sup> Maciej Lewenstein,<sup>1,2</sup> Erez Zohar,<sup>3</sup> Paolo Stornati,<sup>1</sup> and Philipp Hauke<sup>4,5</sup>

<sup>1</sup>*ICFO - Institut de Ciències Fòniques, The Barcelona Institute of Science and Technology, Av. Carl Friedrich Gauss 3, 08860 Castelldefels (Barcelona), Spain*

<sup>2</sup>*ICREA, Pg. Lluís Companys 23, 08010 Barcelona, Spain*

<sup>3</sup>*Racah Institute of Physics, The Hebrew University of Jerusalem, Givat Ram, Jerusalem 91904, Israel*

<sup>4</sup>*Pitaevskii BEC Center and Department of Physics,*

*University of Trento, Via Sommarive 14, I-38123 Trento, Italy*

<sup>5</sup>*INFN-TIFPA, Trento Institute for Fundamental Physics and Applications, Trento, Italy*

(Dated: May 3, 2024)

Gauge-field configurations with non-trivial topology have profound consequences for the physics of Abelian and non-Abelian gauge theories. Over time, arguments have been gathering for the existence of gauge-field configurations with fractional topological charge, called fractons. Ground-state properties of gauge theories can drastically change in presence of fractons in the path integral. However, understanding the origin of such fractons is usually restricted to semi-classical argumentation. Here, we show that fractons persist in strongly correlated many-body systems, using the multiflavor Schwinger model of quantum electrodynamics as a paradigm example. Through detailed numerical tensor-network analysis, we find strong fracton signatures even in highly discretized lattice models, at sizes that are implementable on already existing quantum-simulation devices. Our work sheds light on how the non-trivial topology of gauge theories persists in challenging non-perturbative regimes, and it shows a path forward to probing it in table-top experiments.

*Introduction.*—The topology of the vacuum plays a crucial role in some of the most fundamental theories of nature, including gauge field theories [1] and supersymmetric models [2]. It governs the subtle mechanisms behind such phenomena as charge confinement and chiral symmetry breaking, and topological theta vacua [3] are intrinsically connected to the strong CP problem in quantum chromodynamics (QCD) in 3+1D [4]. Vacuum sectors with distinct topological charge arise naturally from gauge-field configurations with different windings. While naive analysis may suggest the relevance of only sectors with integer windings, configurations with deconfined *fractional topological charge*—called *fractons*—can exist [5] and are in fact vital in resolving paradoxes related to non-vanishing gluino condensates in supersymmetric Yang–Mills theory [6]. Similarly, in non-Abelian gauge theories they can explain the mechanisms behind the formation of a fermion condensate where considerations based on only integer topological charges fall short [5]. However, existing insights into the importance of fractons derive from exactly solvable models or semi-classical arguments. It is not clear if and how signatures of fractons persist in non-perturbative regimes of strongly-correlated theories.

In this work, we demonstrate the presence of fractional gauge-field configurations in the full non-perturbative quantum many-body regime of a paradigmatic gauge theory. Our study dives into the Schwinger model of quantum electrodynamics (QED) with two fermionic flavors, which captures the essence of more complicated quantum field theories, such as QCD, in a simpler, more tractable form. The Schwinger model is a well-established paradigm to facilitate insights into phenomena such as charge confinement, topological theta

vacua, and chiral symmetry breaking [7]. A more recent condensed-matter perspective has also revealed new phenomena [8–10] such as quantum many body scars [11–15], disorder-free localization [16, 17], or dynamical topological phase transitions [18–20]. The multi-flavor version permits for flavor-twisted boundary conditions, which fundamentally modify the symmetry properties of the theory. Analytical calculations at perturbatively small fermion mass [5, 21] have shown that these lead to the deconfinement of fractons. They become visible through a non-zero chiral condensate as well as a fractional dependence of the ground state on the topological theta angle.

Based on tensor network (TN) calculations and exact diagonalization, we demonstrate the persistence of these fracton signatures in the non-perturbative regimes of significant rest mass as well as sizeable lattice spacing. In the limit of vanishing rest mass, even coarse lattice discretizations quantitatively recover the perturbative continuum predictions. Our numerics demonstrates the robustness of fractons against strong quantum fluctuations, lattice artifacts, as well as a cutoff on the gauge-field Hilbert space. Leveraging this considerable robustness towards discretization, we propose a variational quantum algorithm for exploring fractons in a qudit quantum simulator, as has recently been demonstrated in trapped ions [22, 23]. Strong fracton signatures can be observed in such a device with already existing resources, and in the future it may enable to proceed into regimes beyond the capacities of classical numerics. Our results thus demonstrate the importance of fractional gauge-field configurations in the non-perturbative regime of strongly-coupled models, and they present a clear avenue for probing them in quantum hardware.

In the following, we give a brief review of how fractional gauge fields arise in the continuum in the presence of flavor-twisted boundary conditions. The main part of this work consists of our numerical calculations, which reveal fractons in non-perturbative regimes of the truncated lattice Schwinger model. After an analysis of discretization effects, we discuss a variational scheme to probe fracton physics on an existing quantum-simulator platform, before presenting our conclusions.

*Fractons in the multi-flavor Schwinger model.*—We consider (1+1)-dimensional QED [24, 25] with  $N$  fermionic flavors, living on a cylinder  $\mathbb{R} \times \mathbb{S}_L$  that is closed in the spatial direction. We denote its circumference as  $L$  and its volume as  $V = \mathbb{R} \times L$ . The continuum action of the theory is (for details, see SM)

$$S = \int_V d^2x \left\{ -\frac{1}{4} F_{\mu\nu}^2 + i \sum_{p=1}^N \bar{\psi}_p \not{D} \psi_p - \sum_{p=1}^N m_p \bar{\psi}_p \psi_p \right\}, \quad (1)$$

where  $D_\mu = \partial_\mu - ieA_\mu$  is the covariant derivative, capturing the gauge-field-matter interactions.

Fractons are gauge-field configurations in the Euclidean path integral for which the topological invariant, the two-dimensional equivalent of the Pontryagin class,

$$\nu_2 = \frac{e}{4\pi} \int_V d^2x \epsilon_{\mu\nu} F_{\mu\nu}, \quad (2)$$

is a fraction. Often, the symmetry group restricts the possible values of  $\nu_2$  to integers, as happens, e.g., for Abelian anyons in condensed-matter systems [26]. For the multi-flavor Schwinger model, deconfined fractons are allowed by the gauge group and thus the model provides an intriguing testbed for probing their properties.

However, even if fractons exist in a given theory they can be difficult to observe. In the multi-flavor Schwinger model, fractons can be revealed by imposing flavour-twisted boundary conditions for the fermionic fields on the spatial circle,  $\psi_p(x+L) = e^{i\alpha_p} \psi_p(x)$ , where  $\alpha_p = 2\pi p/N$ . For this choice of boundary conditions, the fractons become visible in the Euclidean path integral [5], thanks to a symmetry that emerges from the explicit violation of flavour symmetry and “large gauge transformation”, see SM. One consequence of the presence of fractons is a change of periodicity of the ground state with respect to the  $\theta$ -angle. Conversely, such an increased periodicity can be used to detect the fractons.

Fractional gauge field configurations also influence specific observables. E.g., the chiral condensate at zero temperature and vanishing fermion mass  $m$  can be calculated through the path-integral partition function  $Z(m)$  as

$$\langle \bar{\psi} \psi \rangle = -\frac{\partial}{\partial m} \ln Z(m)|_{m=0}, \quad Z(m) \propto m^{|\nu_2|N}. \quad (3)$$

From Eq. (3), it follows that a non-zero chiral condensate can only be obtained due to gauge-field configurations

with a fractional topological charge  $\nu_2 = 1/N$ . Thus, the spontaneous formation of a chiral condensate is another fingerprint of the existence of fractons.

By including fractons in the path integral, in the limit of vanishing rest mass one obtains analytic predictions for the full  $L$ -dependent chiral condensate [5]:

$$\langle \bar{\psi} \psi \rangle = \sqrt{\frac{\mu e^\gamma}{16\pi L}} e^{-I(L,\mu)/2}, \quad (4)$$

with  $\mu^2 = Ne^2/\pi$  the photon mass,  $\gamma$  Euler’s constant, and  $I(L,\mu)$  a Bessel function given in the SM.

The above analysis holds strictly speaking for the continuum Schwinger model in the exactly solvable limit  $m/e \ll 1$ . It is not a priori clear that a non-perturbative regime will exhibit the same physics. For example, in the opposite limit of  $e/m \ll 1$ , the gauge and matter sectors decouple. Chiral condensation then occurs not due to fractons but due to an explicit breaking of chiral symmetry. This motivates the question how the role of fractons persists into the non-perturbative regime of intermediate couplings  $e/m$ . Similarly, it remains open whether signatures of fractons carry over to strongly-interacting many-body lattice versions of the Schwinger model. As an additional complication of such lattice models, they typically employ a finite cutoff on the gauge-field Hilbert space. This cutoff makes it impossible to define a vector potential (analogous to the difficulties in defining a phase operator) [27], and thus obstructs arguments relying on windings of gauge fields.

In this letter, we dedicate our effort on answering: Can we find signatures for fracton contribution to the ground state physics of a non-perturbative many-body system, and in particular one that can be implemented in present days quantum hardware?

*Truncated lattice Schwinger model.*—To enable numerical simulations in the non-perturbative regime, we employ a lattice Hamiltonian [28] with a cutoff on the Hilbert space of the gauge fields, yielding the truncated Schwinger model (TSM) [29–31]. With two flavors and including the  $\theta$ -angle, its Hamiltonian reads (see SM)

$$\begin{aligned} H_{\text{TSM}} = & \frac{e^2 a}{2} \sum_n (S_n^z)^2 + \frac{e^2 a \theta}{2\pi} \sum_n S_n^z + \frac{e^2 a}{8\pi^2} \theta^2 \\ & + \sum_{n,p} (-1)^{n+p-1} m_p \phi_{n,p}^\dagger \phi_{n,p} \\ & - \frac{i}{2a} \sum_{n,p} (f_{n,p} \phi_{n,p}^\dagger \tilde{S}_n^+ \phi_{n+1,p} - \text{h.c.}). \end{aligned} \quad (5)$$

The coefficient  $f_{n,p}$  is used to implement standard periodic as well as flavor-twisted boundary conditions. The operator  $eS_n^z$  represents the electric field  $E_n$  on link  $n$ .

The operator  $\tilde{S}_n^+$  replaces the unitary parallel transporter  $U_n = \exp(ieA_n)$  by introducing a hard cutoff at  $E_n = \pm S$  (thus leading to the inability mentioned above to define a vector potential). Its matrix elements are given by  $\langle m' | \tilde{S}_n^+ | m \rangle = \delta_{m',m+1}$

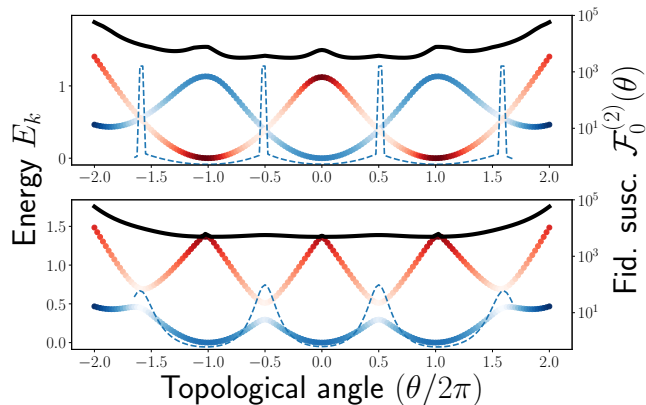


FIG. 1. **Integer vs. fractional  $\theta$ -dependence in the multi-flavor TSM.** Lowest three energy levels of the TSM Hamiltonian for flavor-twisted (upper panel) and flavor-independent (lower panel) boundary conditions, as a function of the  $\theta$ -angle. In the former case, at  $\theta = \pm\pi$ , the two lowest lying states cross and the fidelity susceptibility (blue dotted line) exhibits a strong peak. This indicates a rapid change in the properties of the ground state, suggesting that the periodicity of the ground state is  $4\pi$ . In contrast, in case of flavor-independent boundary conditions avoided crossings occur at  $\theta = \pm\pi$  with only a broad feature in the fidelity susceptibility, rendering the period of each energy level  $2\pi$ .

( $m, m' \in \{-S, \dots, S\}$ ), in contrast to the quantum link model (QLM) [27], where  $S_n^+$  is the usual spin-raising operator with matrix elements  $\langle m' | S_n^+ | m \rangle = \delta_{m', m+1} \sqrt{1 - m(m+1)/[S(S+1)]}$ . As a result, rather than  $[E_n, U_m] = e\delta_{nm}U_m$  and  $[U_n, U_m^\dagger] = 0$ , it obeys the commutation relations

$$[S_n^z, \tilde{S}_m^\pm] = \pm\delta_{nm}\tilde{S}_n^\pm, \quad (6a)$$

$$[\tilde{S}_n^+, \tilde{S}_m^-] = \delta_{nm}(|S\rangle\langle S| - |-S\rangle\langle -S|) \quad (6b)$$

Notably, Eq. (6b) differs from zero only at the cutoff levels of the electric field. Even though the commutators do not smoothly converge to those of lattice Schwinger model as for the QLM [31], one may thus speculate that the TSM captures well the low-energy properties of the (untruncated) lattice Schwinger model, something that we indeed confirm below. To quantify the deviation from the lattice Schwinger model, we introduce

$$\Delta U^2 = \sum_n \langle [\tilde{S}_n^+, \tilde{S}_n^-]^2 \rangle = \sum_n \langle P_n^{(-S)} + P_n^{(+S)} \rangle, \quad (7)$$

where  $P^{(m)} = |m\rangle\langle m|$ . This quantity essentially measures how strongly the link operator fails to be unitary, and is applicable in any dimension and with arbitrary number of flavors.

In the following, we present compelling evidence for the presence of fractons in the TSM already at small truncations ( $S \geq 2$ ). Furthermore, we will show that for  $S \geq 3$  the chiral condensate in the ground state of the

TSM coincides with the semi-classical continuum prediction, with deviations correlated with the strength of the quantity defined in Eq. (7).

*Numerical results.*—Our numerical simulations are based on exact diagonalization (ED) [with system sizes up to  $L = (4 \text{ sites} + 4 \text{ links})$  and truncation up to  $S = 2$ ] and tensor networks (TN) [with up to  $L = (20 \text{ sites} + 20 \text{ links})$  and  $S = 3$ ], see SM for details.

To obtain a direct evidence for fractons in the TSM, we study the lowest energy states as a function of the topological  $\theta$ -angle. For small non-zero fermionic mass,  $m_p = m \neq 0$ , continuum path-integral calculations predict the  $N$  lowest energy levels of the  $N$ -flavor Schwinger model to oscillate as a function of the  $\theta$ -angle as [21]

$$E_k(\theta) = -2m \exp\left(-\frac{\pi}{N\mu eL}\right) \cos\left(\frac{\theta + 2\pi k}{N}\right), \quad (8)$$

where  $k \in \{0, \dots, N-1\}$ . That is, the fracton configurations become manifest through a  $2\pi$  periodicity of  $\theta/N$ , rather than only  $\theta$  as one is used to from the single-flavor Schwinger model. This fractional  $\theta$ -dependence is the precise signature we are looking for.

In Fig. 1, we compare the three lowest energy levels of the TSM as a function of the topological  $\theta$ -angle for flavor-twisted (upper panel) and flavor-independent (lower panel) boundary conditions. We observe a clear gap closing at the points  $\theta = \pm\pi$ , which suggests that ground and first excited state switch roles in a non-adiabatic fashion. To corroborate this result, we compute the fidelity susceptibility [32–34] of the ground state. As the delta-like peak shows, at  $\theta = \pm\pi$  the properties of the ground state change rapidly, indicating a true level crossing. In accordance with Eq. (8), this implies a fractional  $\theta$ -dependence of the ground state. In contrast, for flavor-independent boundary conditions, the gap remains non-zero even at  $\theta = \pm\pi$ . Accordingly, the fidelity susceptibility shows only a broad peak at these points, indicating no drastic property change in the ground state, in accordance with an integer  $\theta$ -dependence. Remarkably, the fracton signature derived from perturbative continuum calculations in the small- $m$  limit persists in a wide range of values of Hamiltonian parameters, including significant rest mass, small system sizes, small gauge-field cutoffs, and large lattice spacing (parameters used in the figure:  $m/e = 0.4$ ,  $L = (4 \text{ sites} + 4 \text{ links})$ ,  $S = 2$ , and  $ea = 1$ ).

*Tensor network calculation of the chiral condensate.*—We obtain further evidence for the presence of fracton configurations by investigating the chiral condensate, which on the lattice with staggered fermions becomes

$$\langle \bar{\psi}\psi \rangle = \frac{1}{L} \sum_n (-1)^n \hat{\phi}_n^\dagger \hat{\phi}_n \quad (9)$$

(here, we suppressed the flavor index). Figure 2 displays the main results of our TN simulations, for the

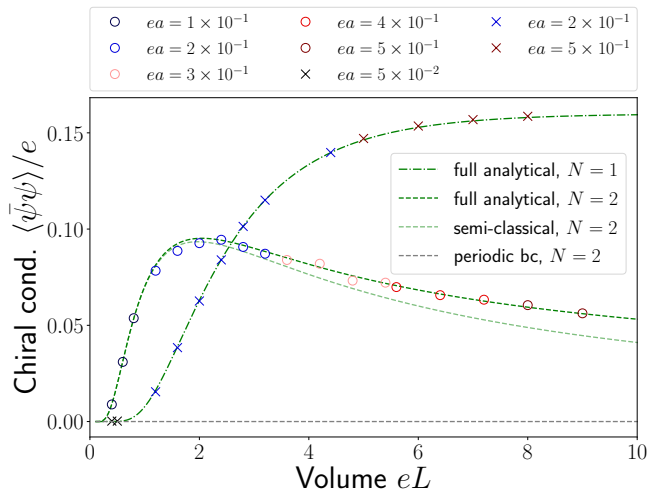


FIG. 2. **Chiral condensate as a fingerprint of fractons in the zero-mass limit.** Throughout a large range of volumes, the TN expectation values of the chiral condensate for the TSM (cutoff  $S = 3$ ) coincide with the analytic predictions from the continuum Schwinger model. This result holds true also beyond the semi-classical approximation and is robust with respect to the lattice discretization and gauge-field cutoff. For a single flavor, a chiral condensate appears due to the chiral anomaly. In the case of two flavors with standard boundary conditions, chiral symmetry is preserved in the ground state. With flavor-twisted boundary conditions, a chiral condensate is allowed and generated by the presence of fractons.

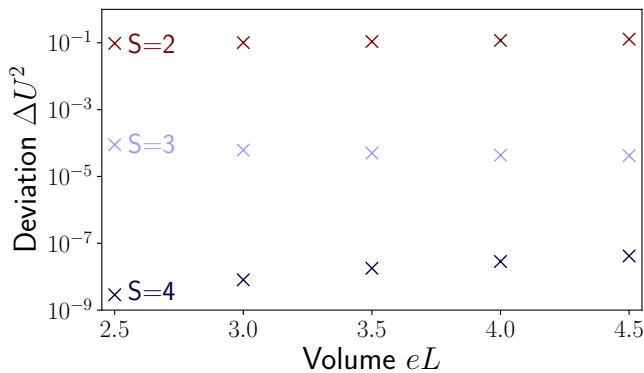


FIG. 3. **Effect of finite gauge-field cutoff.** For very small gauge-field truncations, the violation of the unitarity of the link operator, measured through Eq. (7), is sizeable, but already for  $S = 3$  this deviation falls below a permille. The data suggests an exponential improvement with the cutoff size. (Data for the ground state of the TSM from TN calculations for  $m = 0$  and  $ea = 0.25$ ).

range of physical volume  $eL \in [0.4, 9.0]$ , lattice spacings  $ea \in [0.1, 0.5]$ , and spin truncation  $S = 3$ . As the flavor-twisted boundary conditions induce chiral symmetry breaking, a finite volume can support a non-vanishing chiral condensate. Quite surprisingly, even for the coarse truncation of  $S = 3$ , we encounter throughout the en-

tire range of volumes considered a quantitative agreement between the lattice calculations and the analytical predictions for the continuum Schwinger model [5]. The insignificance of lattice artifacts on the chiral condensate is quite remarkable, considering we do not take the continuum limit [35] and that lattice spacings used are as large as  $ea = 0.5$ .

The same analysis can be made for the single-flavor Schwinger model. Again, the lattice results with  $S = 3$  and  $ea \leq 0.5$  already essentially coincide with the continuum prediction. The single-flavor Schwinger model explicitly breaks chiral symmetry, leading to convergence of the chiral condensate to a non-zero value at  $eL \rightarrow \infty$ . In contrast, for the two-flavor model with standard boundary conditions chiral symmetry is preserved. Flavor-twisted boundary conditions break this symmetry weakly and induce the formation of a chiral condensate, but its strength falls off with  $L$ , highlighting the fact that the effect of boundary conditions disappears for infinite volume. As considerations based on the path integral show [Eq. (3)], the presence of a chiral condensate at vanishing rest mass reveals the contributions due to configurations with fractional topological charge.

Finally, Eq. (7) allows us to monitor finite cutoff errors in the TSM. In Fig. 3, we show  $\Delta U^2$  in a range of lattice volumes for cutoffs  $S = 2, 3, 4$ . Already for  $S = 3$ , the occupation of the cutoff levels of the gauge fields is below a permille. The data suggests a suppression of the error that is exponential in the cutoff, thus leading to a rapid restoration of the commutation relations of the Schwinger model.

*Quantum simulation.*—In recent years, quantum simulators are rapidly evolving to access more and more complex gauge-theory phenomena [36–39], since recently also including the multiflavor Schwinger model [40]. As we show now, existing quantum-simulation technology can probe the physics discussed above, and thus provide a direct demonstration of fractons in an experimental setting. A promising route is via adapting the VQE protocol of Ref. [41] to a qudit quantum processor [22]. The protocol can target the ground state of the multi-flavor TSM by mapped it onto a spin Hamiltonian as in Refs. [42–44]. Thanks to the locality of the resulting Hamiltonian [44], the number of measurements for accurate estimation of the energy will scale only linearly with system size. As it was shown in Ref. [44] for the single-flavor lattice Schwinger model, already shallow variational circuits composed of operations that are native on the trapped-ion qudit platform (single qudit rotations plus entangling Mølmer-Sørensen gates) provide a high-fidelity parametrization of the ground state. Notably, in a trapped-ion quantum simulator the necessary closed boundary conditions can be easily encoded in the variational ansatz due to the all-to-all connectivity. As the above numerical analysis illustrates, already system sizes as small as  $L = (4 \text{ sites} + 4 \text{ links})$  are sufficient for

observing a fractional  $\theta$ -dependence and chiral condensation. These sizes map to 4 qubits + 4 qudits, fitting perfectly into already existing hardware [22]. Moreover, since already very coarse truncations of the electric field are sufficient, the dimensionality of the qudits can be as small as  $d = 5$  ( $S = 2$ ) for qualitative signatures and as small as  $d = 7$  ( $S = 3$ ) for quantitative agreement with continuum results.

*Conclusions.*—In this letter, we investigated fractional gauge field configurations—a version of instantons with a fractional topological charge—and how they contribute to the build-up of a chiral condensate in the multi-flavor Schwinger model. Going beyond semi-classical approximations [5], we have demonstrated the presence of fractons in a strongly-correlated many-body lattice model for various system sizes and in a range of values for the mass and the coupling constant. We have identified the smallest spin truncation ( $S = 3$ ), for which the results for the chiral condensate in the zero-mass limit agree quantitatively with the predictions from the continuum theory. The fingerprints of fractons are thus remarkably robust against non-perturbative effects and discretization and truncation artifacts. As we have argued, this robustness makes it possible to experimentally observe fracton signatures in already existing quantum simulators.

In this work, we have restricted our analysis to two flavors coupled to a  $U(1)$  gauge field. Immediate extensions could investigate large number of fermionic flavors—a testbed for probing phenomena like chiral phase transition in QCD [45–47]. Even though we have revealed signatures of gauge configurations with fractional topological charge in non-perturbative settings, understanding their origin beyond semi-classical arguments remains a long-standing problem. A future research direction could be to develop a characterization in terms of topological invariants valid for an interacting many-body system with local gauge symmetry, in analogy to a similar effort in condensed matter systems [48–50].

## ACKNOWLEDGEMENT

We acknowledge useful discussions with Martin Ringbauer, Matteo Wauters, Emanuele Tirrito, and Niccolò Baldelli.

ICFO group acknowledges support from: ERC AdG NOQIA; MCIN/AEI (PGC2018-0910.13039/501100011033, CEX2019-000910-S/10.13039/501100011033, Plan National FIDEUA PID2019-106901GB-I00, Plan National STAMEENA PID2022-139099NB-I00 project funded by MCIN/AEI/10.13039/501100011033 and by the “European Union NextGenerationEU/PRTR” (PRTR-C17.I1), FPI); QUANTERA MAQS PCI2019-111828-2); QUANTERA DYNAMITE PCI2022-132919 (QuantERA II Programme co-funded by European Union’s

Horizon 2020 program under Grant Agreement No 101017733), Ministry for Digital Transformation and of Civil Service of the Spanish Government through the QUANTUM ENIA project call - Quantum Spain project, and by the European Union through the Recovery, Transformation and Resilience Plan - NextGenerationEU within the framework of the Digital Spain 2026 Agenda; Fundació Cellex; Fundació Mir-Puig; Generalitat de Catalunya (European Social Fund FEDER and CERCA program, AGAUR Grant No. 2021 SGR 01452, QuantumCAT U16-011424, co-funded by ERDF Operational Program of Catalonia 2014-2020); Barcelona Supercomputing Center MareNostrum (FI-2023-1-0013); EU Quantum Flagship (PASQuanS2.1, 101113690, funded by the European Union. Views and opinions expressed are however those of the author(s) only and do not necessarily reflect those of the European Union or the European Commission. Neither the European Union nor the granting authority can be held responsible for them); EU Horizon 2020 FET-OPEN OPTologic (Grant No 899794); EU Horizon Europe Program (Grant Agreement 101080086 — NeQST), results incorporated in this standard have received funding from the European Innovation Council and SMEs Executive Agency under the European Union’s Horizon Europe programme), ICFO Internal “QuantumGaudi” project; European Union’s Horizon 2020 program under the Marie Skłodowska-Curie grant agreement No 847648; “La Caixa” Junior Leaders fellowships, La Caixa” Foundation (ID 100010434): CF/BQ/PR23/11980043. Views and opinions expressed are, however, those of the author(s) only and do not necessarily reflect those of the European Union, European Commission, European Climate, Infrastructure and Environment Executive Agency (CINEA), or any other granting authority. Neither the European Union nor any granting authority can be held responsible for them.

P.P.P. acknowledges also support from the “Secretaria d’Universitats i Recerca del Departament de Recerca i Universitats de la Generalitat de Catalunya” under grant 2024 FI-3 00390, as well as the European Social Fund Plus.

P.H. has received funding from the European Union’s Horizon Europe research and innovation programme under grant agreement No 101080086 NeQST and the Italian Ministry of University and Research (MUR) through the FARE grant for the project DAVNE (Grant R20PEX7Y3A). This project was funded within the QuantERA II Programme that has received funding from the European Union’s Horizon 2020 research and innovation programme under Grant Agreement No 101017733, by the European Union under NextGenerationEU, PRIN 2022 Prot. n. 2022ATM8FY (CUP: E53D23002240006), by the European Union under NextGenerationEU via the ICSC – Centro Nazionale di Ricerca in HPC, Big Data and Quantum Computing, by the Provin-

cia Autonoma di Trento, and Q@TN, the joint lab between University of Trento, FBK—Fondazione Bruno Kessler, INFN—National Institute for Nuclear Physics, and CNR—National Research Council. Views and opinions expressed are however those of the author(s) only and do not necessarily reflect those of the European Union, The European Research Executive Agency, or the European Commission. Neither the European Union nor the granting authority can be held responsible for them.

E.Z. acknowledges the support of the Israel Science Foundation (grant No. 523/20).

---

\* [pavel.popov@icfo.eu](mailto:pavel.popov@icfo.eu)

- [1] Y. Nambu and G. Jona-Lasinio, Dynamical model of elementary particles based on an analogy with superconductivity. i, *Phys. Rev.* **122**, 345 (1961).
- [2] D. Amati, K. Konishi, Y. Meurice, G. C. Rossi, and G. Veneziano, Nonperturbative Aspects in Supersymmetric Gauge Theories, *Phys. Rept.* **162**, 169 (1988).
- [3] A. A. Belavin, A. M. Polyakov, A. S. Schwartz, and Y. S. Tyupkin, Pseudoparticle Solutions of the Yang-Mills Equations, *Phys. Lett. B* **59**, 85 (1975).
- [4] S. M. Barr, D. Chang, and G. Senjanović, Strong cp problem and parity, *Phys. Rev. Lett.* **67**, 2765 (1991).
- [5] M. A. Shifman and A. V. Smilga, Fractons in the twisted multiflavor schwinger model, *Phys. Rev. D* **50**, 7659 (1994).
- [6] N. M. Davies, T. J. Hollowood, V. V. Khoze, and M. P. Mattis, Gluino condensate and magnetic monopoles in supersymmetric gluodynamics, *Nuclear Physics B* **559**, 123 (1999).
- [7] K. Melnikov and M. Weinstein, Lattice schwinger model: Confinement, anomalies, chiral fermions, and all that, *Phys. Rev. D* **62**, 094504 (2000).
- [8] L. Funcke, K. Jansen, and S. Kühn, Topological vacuum structure of the schwinger model with matrix product states, *Physical Review D* **101**, 054507 (2020).
- [9] S. Kühn, J. I. Cirac, and M.-C. Bañuls, Quantum simulation of the schwinger model: A study of feasibility, *Phys. Rev. A* **90**, 042305 (2014).
- [10] G. Magnifico, M. Dalmonte, P. Facchi, S. Pascazio, F. V. Pepe, and E. Ercolessi, Real time dynamics and confinement in the  $\mathbb{Z}_n$  schwinger-weyl lattice model for  $1+1$  qd, *Quantum* **4**, 281 (2020).
- [11] T. Chanda, J. Zakrzewski, M. Lewenstein, and L. Tagliacozzo, Confinement and lack of thermalization after quenches in the bosonic schwinger model, *Phys. Rev. Lett.* **124**, 180602 (2020).
- [12] D. Banerjee and A. Sen, Quantum scars from zero modes in an abelian lattice gauge theory on ladders, *Phys. Rev. Lett.* **126**, 220601 (2021).
- [13] J. C. Halimeh, L. Barbiero, P. Hauke, F. Grusdt, and A. Bohrdt, Robust quantum many-body scars in lattice gauge theories, *Quantum* **7**, 1004 (2023).
- [14] I. Sau, P. Stornati, D. Banerjee, and A. Sen, Sublattice scars and beyond in two-dimensional  $u(1)$  quantum link lattice gauge theories, *Phys. Rev. D* **109**, 034519 (2024).
- [15] J.-Y. Desaulles, A. Hudomal, D. Banerjee, A. Sen, Z. Papić, and J. C. Halimeh, Prominent quantum many-body scars in a truncated schwinger model, *Phys. Rev. B* **107**, 205112 (2023).
- [16] M. Brenes, M. Dalmonte, M. Heyl, and A. Scardicchio, Many-body localization dynamics from gauge invariance, *Phys. Rev. Lett.* **120**, 030601 (2018).
- [17] H. Lang, P. Hauke, J. Knolle, F. Grusdt, and J. C. Halimeh, Disorder-free localization with stark gauge protection, *Phys. Rev. B* **106**, 174305 (2022).
- [18] T. V. Zache, N. Mueller, J. T. Schneider, F. Jendrzejewski, J. Berges, and P. Hauke, Dynamical topological transitions in the massive schwinger model with a  $\theta$  term, *Phys. Rev. Lett.* **122**, 050403 (2019).
- [19] N. Mueller, J. A. Carolan, A. Connelly, Z. Davoudi, E. F. Dumitrescu, and K. Yeter-Aydeniz, Quantum computation of dynamical quantum phase transitions and entanglement tomography in a lattice gauge theory, *PRX Quantum* **4**, 030323 (2023).
- [20] D. Pomarico, L. Cosmai, P. Facchi, C. Lupo, S. Pascazio, and F. V. Pepe, Dynamical quantum phase transitions of the schwinger model: Real-time dynamics on ibm quantum, *Entropy* **25**, 10.3390/e25040608 (2023).
- [21] T. Misumi, Y. Tanizaki, and M. Ünsal, Fractional  $\theta$  angle, 't hooft anomaly, and quantum instantons in charge- $q$  multi-flavor schwinger model, *Journal of High Energy Physics* **2019**, 1 (2019).
- [22] M. Ringbauer, M. Meth, L. Postler, R. Stricker, R. Blatt, P. Schindler, and T. Monz, A universal qudit quantum processor with trapped ions, *Nature Physics* **18**, 1053 (2022).
- [23] M. Meth, J. F. Haase, J. Zhang, C. Edmunds, L. Postler, A. Steiner, A. J. Jena, L. Dellantonio, R. Blatt, P. Zoller, *et al.*, Simulating 2d lattice gauge theories on a qudit quantum computer, arXiv preprint arXiv:2310.12110 (2023).
- [24] J. Schwinger, Gauge invariance and mass. ii, *Phys. Rev.* **128**, 2425 (1962).
- [25] J. Schwinger, The theory of quantized fields. i, *Phys. Rev.* **82**, 914 (1951).
- [26] C. Nayak, S. H. Simon, A. Stern, M. Freedman, and S. Das Sarma, Non-abelian anyons and topological quantum computation, *Rev. Mod. Phys.* **80**, 1083 (2008).
- [27] S. Chandrasekharan and U.-J. Wiese, Quantum link models: A discrete approach to gauge theories, *Nucl. Phys. B* **492**, 455 (1997).
- [28] J. Kogut and L. Susskind, Hamiltonian formulation of Wilson's lattice gauge theories, *Phys. Rev. D* **11**, 395 (1975).
- [29] E. Zohar, J. I. Cirac, and B. Reznik, Simulating compact quantum electrodynamics with ultracold atoms: Probing confinement and nonperturbative effects, *Phys. Rev. Lett.* **109**, 125302 (2012).
- [30] J.-Y. Desaulles, A. Hudomal, D. Banerjee, A. Sen, Z. Papić, and J. C. Halimeh, Prominent quantum many-body scars in a truncated schwinger model, *Phys. Rev. B* **107**, 205112 (2023).
- [31] J.-Y. Desaulles, E. J. Gustafson, A. C. Li, Z. Papić, and J. C. Halimeh, Robust finite-temperature many-body scarring on a quantum computer, arXiv preprint arXiv:2309.11543 (2023).
- [32] S.-J. Gu, Fidelity approach to quantum phase transitions, *International Journal of Modern Physics B* **24**, 4371 (2010).
- [33] P. Hauke, F. M. Cucchietti, A. Müller-Hermes, M.-C. Bañuls, J. I. Cirac, and M. Lewenstein, Complete devil's

- staircase and crystal–superfluid transitions in a dipolar xxz spin chain: a trapped ion quantum simulation, *New Journal of Physics* **12**, 113037 (2010).
- [34] L. Wang, Y.-H. Liu, J. Imriška, P. N. Ma, and M. Troyer, Fidelity susceptibility made simple: A unified quantum monte carlo approach, *Phys. Rev. X* **5**, 031007 (2015).
- [35] M. C. Bañuls, K. Cichy, K. Jansen, and H. Saito, Chiral condensate in the schwinger model with matrix product operators, *Phys. Rev. D* **93**, 094512 (2016).
- [36] M. C. Bañuls *et al.*, Simulating lattice gauge theories within quantum technologies, *Eur. Phys. J. D* **74** (2020).
- [37] M. Aidelsburger, L. Barbiero, A. Bermudez, T. Chanda, A. Dauphin, D. González-Cuadra, P. R. Grzybowski, S. Hands, F. Jendrzejewski, J. Jünemann, *et al.*, Cold atoms meet lattice gauge theory, *Philosophical Transactions of the Royal Society A* **380**, 20210064 (2022).
- [38] D. Beck, J. Carlson, Z. Davoudi, J. Formaggio, S. Quaglioni, M. Savage, J. Barata, T. Bhattacharya, M. Bishof, I. Cloet, A. Delgado, M. DeMarco, C. Fink, A. Florio, M. Francois, D. Grabowska, S. Hoogerheide, M. Huang, K. Ikeda, M. Illa, K. Joo, D. Kharzeev, K. Kowalski, W. K. Lai, K. Leach, B. Loer, I. Low, J. Martin, D. Moore, T. Mehen, N. Mueller, J. Mulligan, P. Mumm, F. Pederiva, R. Pisarski, M. Ploskon, S. Reddy, G. Rupak, H. Singh, M. Singh, I. Stetcu, J. Stryker, P. Szypryt, S. Valgushev, B. VanDevender, S. Watkins, C. Wilson, X. Yao, A. Afanasev, A. B. Balantekin, A. Baroni, R. Bunker, B. Chakraborty, I. Chernyshev, V. Cirigliano, B. Clark, S. K. Dhiman, W. Du, D. Dutta, R. Edwards, A. Flores, A. Galindo-Uribarri, R. F. G. Ruiz, V. Gueorguiev, F. Guo, E. Hansen, H. Hernandez, K. Hattori, P. Hauke, M. Hjorth-Jensen, K. Jankowski, C. Johnson, D. Lacroix, D. Lee, H.-W. Lin, X. Liu, F. J. Llanes-Estrada, J. Looney, M. Lukin, A. Mercenne, J. Miller, E. Mottola, B. Mueller, B. Nachman, J. Negele, J. Orrell, A. Patwardhan, D. Phillips, S. Poole, I. Qualters, M. Rumore, T. Schaefer, J. Scott, R. Singh, J. Vary, J.-J. Galvez-Viruet, K. Wendt, H. Xing, L. Yang, G. Young, and F. Zhao, Quantum information science and technology for nuclear physics. input into u.s. long-range planning, 2023 (2023), [arXiv:2303.00113](https://arxiv.org/abs/2303.00113) [nucl-ex].
- [39] J. C. Halimeh, M. Aidelsburger, F. Grusdt, P. Hauke, and B. Yang, Cold-atom quantum simulators of gauge theories (2023), [arXiv:2310.12201](https://arxiv.org/abs/2310.12201) [cond-mat.quant-gas].
- [40] L. Funcke, T. Hartung, K. Jansen, S. Kühn, M.-O. Pleinert, S. Schuster, and J. von Zanthier, Exploring the phase structure of the multi-flavor schwinger model with quantum computing (2022), [arXiv:2211.13020](https://arxiv.org/abs/2211.13020) [quant-ph].
- [41] C. Kokail, C. Maier, R. van Bijnen, T. Brydges, M. K. Joshi, P. Jurcevic, C. A. Muschik, P. Silvi, R. Blatt, C. F. Roos, and P. Zoller, Self-verifying variational quantum simulation of lattice models, *Nature* **569**, 355 (2019).
- [42] E. Zohar and J. I. Cirac, Eliminating fermionic matter fields in lattice gauge theories, *Phys. Rev. B* **98**, 075119 (2018).
- [43] E. Zohar and J. I. Cirac, Removing staggered fermionic matter in  $u(n)$  and  $su(n)$  lattice gauge theories, *Phys. Rev. D* **99**, 114511 (2019).
- [44] P. P. Popov, M. Meth, M. Lewenstein, P. Hauke, M. Ringbauer, E. Zohar, and V. Kasper, Variational quantum simulation of  $u(1)$  lattice gauge theories with qudit systems, *Phys. Rev. Res.* **6**, 013202 (2024).
- [45] R. D. Pisarski and F. Wilczek, Remarks on the chiral phase transition in chromodynamics, *Phys. Rev. D* **29**, 338 (1984).
- [46] Y. Aoki, G. Endrődi, Z. Fodor, S. D. Katz, and K. K. Szabó, The order of the quantum chromodynamics transition predicted by the standard model of particle physics, *Nature* **443**, 675–678 (2006).
- [47] J. Wu, C. Li, Y. Wang, and T. Wumaier, Exploring the enigmatic chiral phase transition of qcd at finitetemperature (2024), [arXiv:2401.17970](https://arxiv.org/abs/2401.17970) [hep-th].
- [48] Z. Wang and S.-C. Zhang, Simplified topological invariants for interacting insulators, *Phys. Rev. X* **2**, 031008 (2012).
- [49] A. Elben, J. Yu, G. Zhu, M. Hafezi, F. Pollmann, P. Zoller, and B. Vermersch, Many-body topological invariants from randomized measurements in synthetic quantum matter, *Science Advances* **6**, 10.1126/sciadv.aaz3666 (2020).
- [50] L. Lin, Y. Ke, and C. Lee, Topological invariants for interacting systems: From twisted boundary conditions to center-of-mass momentum, *Phys. Rev. B* **107**, 125161 (2023).
- [51] S. R. Coleman, There are no Goldstone bosons in two-dimensions, *Commun. Math. Phys.* **31**, 259 (1973).
- [52] F. Berruto, G. Grignani, G. W. Semenoff, and P. Sodano, Spectrum of the two-flavor schwinger model from the heisenberg spin chain, *Phys. Rev. D* **59**, 034504 (1999).
- [53] R. Dempsey, I. R. Klebanov, S. S. Pufu, and B. Zan, Discrete chiral symmetry and mass shift in the lattice hamiltonian approach to the schwinger model, *Phys. Rev. Res.* **4**, 043133 (2022).

## SUPPLEMENTAL MATERIAL

### Lagrange formulation, path integral of the Schwinger model, and fractional gauge configurations

In this section, we briefly summarize the main notation useful for understanding the path integral formulation of QED in (1+1) dimensions. We also explain how fractons arise in the Euclidean path integral of this theory. The Lagrange density of the multi-flavor Schwinger model, including the topological  $\theta$ -angle, on a torus  $\mathbb{T} = \mathbb{S}_\beta \times \mathbb{S}_L$ , where  $\beta = 1/T$  is the inverse temperature and  $L$  is the spatial volume, reads

$$\begin{aligned} \mathcal{L}_\theta(\mathbf{x}) = & \frac{ie\theta}{4\pi} \epsilon_{\mu\nu} F_{\mu\nu}(\mathbf{x}) - \frac{1}{4} F_{\mu\nu}(\mathbf{x})^2 + \\ & i \sum_{p=1}^{N_f} \bar{\psi}_p(\mathbf{x}) \not{D}(\mathbf{x}) \psi_p(\mathbf{x}) - \sum_{p=1}^{N_f} m_p \bar{\psi}_p(\mathbf{x}) \psi_p(\mathbf{x}), \end{aligned} \quad (10)$$

where  $\mathbf{x} = (\tau, x)$  with  $\tau$  being the Euclidean time. Here, we use Euclidean signature with  $\epsilon_{\mu\nu}$  being the total anti-symmetric tensor in 2 dimensions,  $F_{\mu\nu} = \partial_\mu A_\nu - \partial_\nu A_\mu$  the field strength tensor of the  $U(1)$  gauge field  $A_\mu$ ,  $\psi_p$  the two-component Dirac field of the  $p$ 'th flavor with bare mass  $m_p$ ,  $e$  the coupling constant, and  $N$  the number of flavors. Without loss of generality, the  $\theta$ -angle can be restricted to values in the interval  $\theta \in [0, 2\pi]$ . The Euclidean action is defined as the integral over the volume of the Lagrange density  $S_\theta = \int_{\mathbb{T}} d^2x \mathcal{L}_\theta(\mathbf{x})$ .

The object of central interest is the Euclidean path integral (or the partition function) of the Schwinger model, which is defined as an integral over all configurations for  $\psi$  and  $A_\mu$

$$Z = \int \mathcal{D}A_\mu \mathcal{D}\psi \mathcal{D}\bar{\psi} e^{-S_\theta[\bar{\psi}, \psi, A_\mu]}. \quad (11)$$

In the differential of the integral, a product over the fermion flavors is implied. Via the anomaly, the  $\theta$ -term in the action can be traded for a summation over partition functions  $Z_n$  deriving from sectors with distinct topological charge  $\nu_2 = n$ , i.e.,

$$Z = \sum_n Z_n = \sum_n e^{-in\theta} \int_n \mathcal{D}A_\mu \mathcal{D}\psi \mathcal{D}\bar{\psi} e^{-S[\bar{\psi}, \psi, A_\mu]}. \quad (12)$$

Here,  $S = \int_{\mathbb{T}} d^2x \mathcal{L}_{\theta=0}(\mathbf{x})$  and we use the index  $n$  to denote integration only over gauge-field configurations with specified winding corresponding to topological charge  $n$ .

The topology in the gauge sector is determined by the boundary conditions. Gauge-field configurations with integer topological charge  $\nu_2 = n \in \mathbb{Z}$ , or ‘‘instantons’’, sat-

isfy standard boundary conditions (sbc) in time direction

$$\begin{aligned} A_0(\tau + T, x) &= A_0(\tau, x), \\ A_1(\tau + T, x) &= A_1(\tau, x) + \frac{2\pi n}{eL}, \\ \psi_p(\tau + T, x) &= e^{-2\pi nix/L} \psi_p(\tau, x). \end{aligned} \quad (13)$$

However, this is not the only possible choice for boundary conditions of the gauge fields. In the presence of multiple fermionic flavours, the ‘‘large gauge transformation’’ allows for boundary conditions that correspond to a fractional topological charge  $\nu_2 = m/N$ ,  $m \in \mathbb{Z}$ :

$$\begin{aligned} A_0(\tau + T, x) &= A_0(\tau, x), \\ A_1(\tau + T, x) &= A_1(\tau, x) + \frac{2\pi m}{NeL}, \\ \psi_p(\tau + T, x) &= \psi_{p+1}(\tau, x) \text{ for } p \in \{1, \dots, N-1\}, \\ \psi_N(\tau + T, x) &= e^{-2\pi m ix/L} \psi_1(\tau, x). \end{aligned} \quad (14)$$

The gauge field configurations that satisfy Eq. (14) are called fractons. By including them in the Euclidean path integral, the summation in Eq. (12) is taken over  $n = m/N$ , with  $m \in \mathbb{Z}$ . In contrast, for the single-flavor Schwinger model, the summation is directly over integer  $n \in \mathbb{Z}$ . As Eq. (12) shows, the periodicity with respect to the  $\theta$ -angle increases accordingly to  $N2\pi$ . The existence of fractons can thus modify the properties of the ground state in a profound way.

### Detecting fractons via the chiral condensate in the presence of flavour-twisted boundary conditions

The fractons in the multi-flavour Schwinger model can be revealed by detecting their contribution to observables like the chiral condensate. When flavor-independent (‘‘standard’’) boundary conditions in space direction are imposed on the fermions, i.e.,  $\psi_p(x+L) = e^{i\alpha} \psi_p(x) \forall p \in \{1, \dots, N\}$ , potentially with a flavor-independent phase  $\alpha$ , the system has a  $SU(N)_L \otimes SU(N)_R$  flavor symmetry in the zero mass limit, prohibiting the generation of a chiral condensate due to the Mermin–Wagner–Coleman theorem [51]. However, in case the phase  $\alpha$  is flavor dependent, e.g.,  $\alpha_p = 2\pi p/N$ , the chiral symmetry is explicitly broken and chiral condensation can be allowed even for vanishing rest masses [5].

Semi-classical analytics for small volumes ( $eL \ll 1$ ) as well as exact path-integral calculations at arbitrary volumes [5] (both at vanishing rest mass), show that such flavor-twisted boundary conditions (fbc) indeed result in a non-vanishing chiral condensate. The main ingredient of this analysis is a new symmetry that the ground state obeys under fbc, induced by the ‘‘fractional’’ transforma-



tion

$$\begin{aligned} A_1(x) &\xrightarrow{\text{fbc}} \tilde{\mathcal{S}}[A_1(x)] = A_1(x) + \frac{2\pi}{NeL}, \\ \psi_p(x) &\xrightarrow{\text{fbc}} \tilde{\mathcal{S}}[\psi_p(x)] = e^{-i\frac{2\pi x}{NL}} \psi_{p+1}(x), \end{aligned} \quad (15)$$

in contrast to the symmetry transformation for standard boundary conditions

$$\begin{aligned} A_1(x) &\xrightarrow{\text{sbc}} \mathcal{S}[A_1(x)] = A_1(x) + \frac{2\pi}{eL}, \\ \psi_p(x) &\xrightarrow{\text{sbc}} \mathcal{S}[\psi_p(x)] = e^{-i\frac{2\pi x}{L}} \psi_p(x). \end{aligned} \quad (16)$$

The ‘‘fractional’’ transformation is a combination of broken chiral symmetry and forbidden ‘‘large gauge transformation’’ and has a period  $1/N$  times smaller than for sbc. The existence of this new symmetry requires one to impose a new superselection rule, one in which the length of a noncontractable circle in the space of gauge fields is reduced by the number of flavors  $N$ . On the level of the path integral, this symmetry leads to the increased  $\theta$ -periodicity discussed in the previous section.

Exploiting this symmetry, path-integral calculations that are possible in the limit of vanishing rest mass lead to the analytic predictions for the  $L$ -dependent chiral condensate [5], as given in the main text:

$$\langle \bar{\psi}\psi \rangle = \sqrt{\frac{\mu e^\gamma}{16\pi L}} e^{-I(L,\mu)/2}, \quad (17)$$

with  $\mu^2 = Ne^2/\pi$  the photon mass,  $\gamma$  Euler’s constant, and

$$I = \int_0^\infty \frac{d\omega}{\sqrt{\omega^2 + \mu^2}} \left( \coth \frac{L\sqrt{\omega^2 + \mu^2}}{2} - 1 \right). \quad (18)$$

### Lattice Hamiltonian

To make the continuum theory suitable for the simulation techniques developed for many-body systems, we formulate it as a lattice Hamiltonian [28]. On the lattice, the local symmetry of the continuum model translates into local constraints of the Hilbert space of matter and gauge fields. States are considered physical if they obey the Gauss’s law  $G_n |\psi\rangle = 0$ , where

$$G_n = E_n - E_{n-1} - e \sum_p \phi_{n,p}^\dagger \phi_{n,p}. \quad (19)$$

In view of implementation in a numerical or quantum simulation, we further truncate the infinite Hilbert space of each gauge field. One common possibility is the Quantum Link Model [27] representation, where the local Hilbert space on each link is given by that of a spin- $S$  object. In that formulation of quantum electrodynamics, the electric field operator  $E_n$  on a link is replaced by the

spin- $Z$  operator  $eS_n^Z$ ; the link operator (parallel transporter)  $U = \exp ieA_n$ , which describes the dynamical Peierls phase picked up by a fermion moving from lattice site  $n$  to  $n+1$  and which raises the electric field by one unit, is replaced by  $[S(S+1)]^{-1/2} S_n^+$ . Here, instead, we consider the so-called truncated Schwinger model (TSM) [29–31], where  $U$  is replaced by the operator  $\tilde{S}_n^+$ , whose matrix elements are given by  $[\tilde{S}^+]_{i,j} := \delta_{j,i+1}$ , up to a sharp cutoff at  $\pm S$ .

With two flavors, the Hamiltonian of the TSM, including the  $\theta$ -angle, reads

$$\begin{aligned} H_{\text{TSM}} &= \frac{e^2 a}{2} \sum_n (S_n^z)^2 + \frac{e^2 a \theta}{2\pi} \sum_n S_n^z + \frac{e^2 a}{8\pi^2} \theta^2 \\ &+ \sum_{n,p} (-1)^{n+p-1} m_p \phi_{n,p}^\dagger \phi_{n,p} \\ &- \frac{i}{2a} \sum_{n,p} (f_{n,p} \phi_{n,p}^\dagger \tilde{S}_n^+ \phi_{n+1,p} - \text{h.c.}). \end{aligned} \quad (20)$$

The first term represents the electric field energy and the second the topological  $\theta$ -angle, equivalent to a background field. We also included a constant proportional to  $\theta^2$  in order to be able to more clearly compare ground-state energies at different  $\theta$ -angles. The term in the second line represents the fermionic rest masses. Here, we use staggered fermions and chose to stagger the two flavors in opposite ways. Namely, the first flavor’s particles (anti-particles) live on even (odd) sites, and opposite for the second flavor. This trick allows us to preserve a discrete chiral symmetry on the lattice, present in the continuum Schwinger model [52, 53]. Finally, the third line represents the fermionic kinetic energy, which is coupled to the gauge field. For  $f_{n,p} \equiv 1$ , the system is under sbc, while  $f_{n,p} = -1$ , if  $n = L$  and  $p = 2$  and  $+1$  otherwise implements the flavor-twisted boundary conditions in our many-body lattice model.

### Numerical implementation

Our numerical simulations are based on two techniques: exact diagonalization (ED) using the QuSpin package in Python, employed for system sizes up to  $L = (4 \text{ sites} + 4 \text{ links})$ , with a spin  $1/2$  on each site and up to spin  $3$  on each link; and tensor network (TN) calculations using ITensors in Julia, with system sizes up to  $L = (20 \text{ sites} + 20 \text{ links})$  and similar spin sizes as for ED. For the TN calculations, the maximal bond dimension used in the MPS representation of the variational state is  $\chi_{\text{max}} = 500$ , which we found sufficient for obtaining converged results. In our numerical simulations, we implement the dimensionless version [35] of the Hamiltonian of Eq. (5) -  $H \rightarrow H/e^2 a$ .

### Fidelity susceptibility

In Fig. 1 of the main text, we show the fidelity susceptibility of the ground state as a function of the  $\theta$ -angle:

$$\mathcal{F}_0^{(2)}(\theta) = \frac{\partial^2}{\partial \delta^2} |\langle \psi(\theta) | \psi(\theta + \delta) \rangle|^2 |_{\delta=0}. \quad (21)$$

This quantity is used to indicate phase transitions and rapid changes of the properties of the corresponding state [32–34]; at an avoided crossing, the fidelity susceptibility shows a broad peak, and at a true level crossing a delta-like peak. In the latter case, the properties of the ground state on the left of the crossing point are drastically different from the ones on the right.

In practice, we compute the discretized version of this quantity

$$\mathcal{F}_0^{(2)}(\theta, \delta) = \frac{1}{\delta^2} [|\langle \psi(\theta) | \psi(\theta + \delta) \rangle|^2 + |\langle \psi(\theta) | \psi(\theta - \delta) \rangle|^2 - 2], \quad (22)$$

for a sufficiently small  $\delta = 0.025$ . Further decrease of  $\delta$  shows a narrowing of the peak and exploding of the amplitude in case of flavor-twisted boundary conditions and no significant change in case of flavor-independent boundary conditions. The fact that the fidelity susceptibility behaves differently for fbc with respect to sbc means that the periodicity in  $\theta$  in the former case is  $4\pi$ , whereas in the later case it is  $2\pi$ .